IJPSR (2021), Volume 12, Issue 4 (Research Article)

INTERNATIONAL JOURNAL OF PHARMACEUTICAL SCIENCES AND RESEARCH

Received on 25 August 2019; received in revised form, 26 February 2021; accepted, 04 March 2021; published 01 April 2021

# PREPARATION AND CHARACTERIZATION OF $Fe_3O_4$@$SiO_2$@L-VALINE NANOPARTICLES AS AN EFFECTIVE AND NOVEL NANOCATALYST FOR THE SYNTHESIS OF PERIMIDINE DERIVATIVE UNDER MILD CONDITIONS

Shadi Siabi [1], Hoda Pasdar [*1], Naser Foroughifar [1], Mehran Davallo [1] and Reza Fazaeli [2]

Department of Chemistry [1], North Tehran Branch, Islamic Azad University, Tehran, 1651153311, Iran.
Department of Chemical Engineering [2], Faculty of Engineering, South Tehran Branch, Islamic Azad University, Tehran, Iran.

**Keywords:**

Perimidine, L-valine, Magnetic Nanoparticles, Recyclable catalyst, Antibacterial activity

**Correspondence to Author:**
**Hoda Pasdar**

Department of Chemistry,
North Tehran Branch, Islamic Azad University, Tehran, 1651153311, Iran.

**E-mail:** h_pasdar@iau-tnb.ac.ir

**ABSTRACT:** We presented an eco-friendly procedure for effective and fast preparation of biologically active substituted pyrimidine ligand through a condensation reaction of 1,8-diaminonaphthalene and 2-methoxy-benzaldehyde with $Fe_3O_4$@$SiO_2$@L-valine magnetic nanoparticles (MNPs) as a new recyclable catalyst. In this experiment, we aim to increase reaction efficiency for the synthesis of 2-(2-methoxyphenyl)-2,3-dihydro-1H-perimidine ligand. Fourier transform infrared (FT-IR) spectroscopy, X-ray diffraction (XRD), Energy dispersive X-ray spectrometer (EDXA), scanning electron microscopy (SEM), and vibrating sample magnetometry (VSM) were employed to characterize the catalyst. Findings demonstrated that synthesized nanocatalyst is superparamagnetic with a dimension range of 15-30 nm. The catalyst was readily recycled using an external magnet and could be recovered several times without considerable reduction in its catalytic performance. Furthermore, the metal complexes were produced from 2-(2-methoxyphenyl)-2,3-dihydro-1H-perimidine ligand. Antibacterial activities of ligand and its metal complexes were studied against G(+) and G(-) bacteria strains by disc diffusion technique. Results showed that metal complexes had better biological activities compared to parent ligands. Among the synthesized compounds, the best antibacterial activity was observed by Cu complex.

**INTRODUCTION:** Nitrogen comprising hetero-cyclic compounds like pyridine, imidazole, and perimidine has a variety of pharmacological properties [1]. Mostly, perimidine derivatives have been of great interest because of their remarkable biological activities such as antifungal, anticancer, antihelmintic, anti-bacterial, antioxidant, antihista-minic and anticancer.

QUICK RESPONSE CODE

DOI: 10.13040/IJPSR.0975-8232.12(4).2385-93

This article can be accessed online on www.ijpsr.com

DOI link: http://dx.doi.org/10.13040/IJPSR.0975-8232.12(4).2385-93

Several pyrimidine derivatives can be synthesized through a condensation reaction of 1,8 diamino-naphthalene and ketones/aldehydes, although merely protonic acids were utilized as catalysts for their production in the past. Their strong acidity, however, could cause several side reactions, and to a small extent, to the substrates, so these compounds are not considered very efficient. There has been a need to find an effective catalyst for these reactions.

In recent years, silica-coated nanoparticles have shown catalytic activity in condensation reaction of 1,8-diaminonaphthalene with aromatic aldehydes [2]. Homogeneous catalysts have more catalytic properties compared to heterogeneous catalysts

owing to their solubility in the reaction environment, which enhances catalytic site availability for the substrate, but their disadvantage is their covering process, which is frequently time-consuming [3, 4]. Moreover, there is the issue of product pollution found when homogeneous catalysts are utilized. On the other hand, heterogeneous catalysts have unique features such as a large surface area to volume ratio, thermal and mechanical constancy, and insolubility in organic and aqueous solutions. [5, 6] Consequently, to overcome the problems of homogeneous catalysts, nano-sized heterogeneous catalysts have been utilized recently in organic synthesis [7, 8].

Magnetic nanoparticles (MNPs) have greatly interested owing to their unique features and diverse applications like magnetic resonance imaging (MRI), drug delivery, and as catalysts in chemical reactions [9, 10]. Nanoparticles are very small in dimension and could be dispersed consistently in the solutions explaining their higher catalyst performance [11]. When a nanoparticle catalyst is well dispersed in the reaction environment, it creates a stable suspension and enhances the rate of reaction [12]. The most challenging problem of applying nanoparticles in organic reactions is that they are not recoverable and their recycling from the reaction solution is not simple. However, MNPs can be simply separated from the reaction environment by means of an external magnet. In the current study, novel $Fe_3O_4$@$SiO_2$@L-valine was synthesized as a recoverable catalyst for synthesizing perimidine derivative. Next, the metal complexes were synthesized from this ligand, and the antibacterial behavior of the prepared compounds was examined against gram-positive and gram-negative bacterial strains.

## RESULTS AND DISCUSSION:

**Synthesis and Characterization of the Catalyst:** In the current research, Fe3O4@SiO2@L-valine MNPs were synthesized as reusable and recyclable catalysts for the first time (**Scheme 1**). In the first phase, the $Fe_3O_4$ MNPs were synthesized through co-precipitation of $Fe^{2+}$ and $Fe^{3+}$ ions. Then, to prevent probable oxidation and aggregation of $Fe_3O_4$ MNPs, these were surface-coated with silica. In the final phase, $Fe_3O_4$@$SiO_2$@L-valine MNPs were synthesized by condensing the reaction of $Fe_3O_4$@$SiO_2$ with L-valine. Characterization of the catalyst was performed by Fourier transform infrared (FT-IR) spectroscopy, X-ray diffraction (XRD), Energy dispersive X-ray analysis (EDXA), scanning electron microscopy (SEM), and vibrating sample magnetometry (VSM).

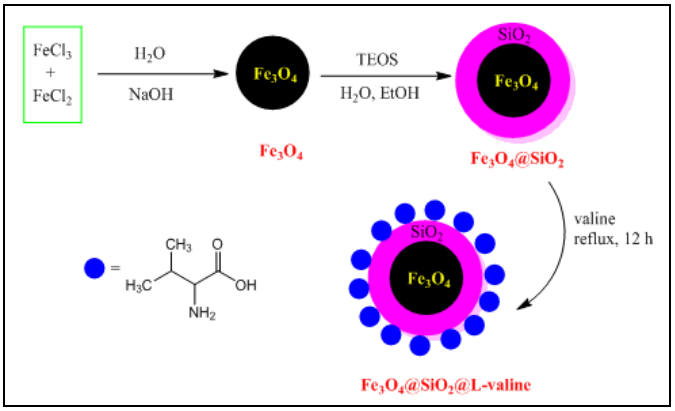


**SCHEME 1: PREPARATION OF $Fe_3O_4$@$SiO_2$@L-VALINE MNPs**

**FTIR Spectroscopy: Fig. 1a** represents the FTIR spectrum corresponding to $Fe_3O_4$ NPs. The stretching vibration at 585 $cm^{-1}$ can be assigned to Fe-O bond of iron oxide. This peak is seen in all three compounds. In the FTIR spectrum corresponding to $Fe_3O_4$@$SiO_2$ **Fig. 1b**, the observed peak at 1092 $cm^{-1}$is related to Si-O bond which approves the preparation of $SiO_2$ shells. The FTIR spectrum corresponding to $Fe_3O_4$@$SiO_2$@L-valine gave bands specific to L-valine, with a strong amide absorption at 1619 $cm^{-1}$. Also, the stretching that appeared at 3380 $cm^{-1}$ was related to the hydroxyl group.

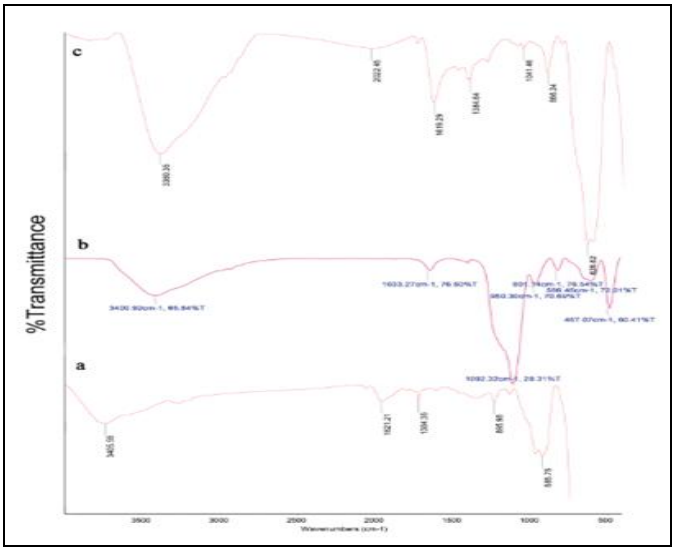


**FIG. 1: FTIR SPECTRUM OF $Fe_3O_4$ (A), $Fe_3O_4$@$SiO_2$(B) AND $Fe_3O_4$@$SiO_2$@L-VALINE (C).**

**XRD Study**: **Fig. 2** shows the XRD patterns corresponding to $Fe_3O_4$ (a), $Fe_3O_4$@$SiO_2$(b), and $Fe_3O_4$@$SiO_2$@L-valine (c) with seven characteristic bands at $2\theta$ = 30.4, 35.7, 43.4, 53.88, 56.4, 63.04, 74.5 which related to the (220), (311), (400), (422), (511), (440) and (533) plans of the $Fe_3O_4$, respectively. This outcome is completely in accordance with the crystalline cubic spinel structure of $Fe_3O_4$ nanoparticles (JCPDS card No. 85-1436). The weak broad peaks at 2θ = 21 in $Fe_3O_4$@$SiO_2$ and $Fe_3O_4$@$SiO_2$@L-valine can be assigned to the presence of amorphous silica around the cores. The mean particle dimension (D) of $Fe_3O_4$@$SiO_2$@L-valine is 20 nm, which was computed by Debye-Scherer formula (Equation 1):

$$D = \frac{k\lambda}{\beta \cos\theta} \qquad \text{Equation (1)}$$

In this equation, D refers to the crystalline dimension, k represents a shape function for which a value of 0.9 was utilized, λ refers to the wavelength of the radiation (0.154 nm), and β represents the full-width at half-maximum (FWHM) in radians in the 2θ scale, and θ the Bragg angle.

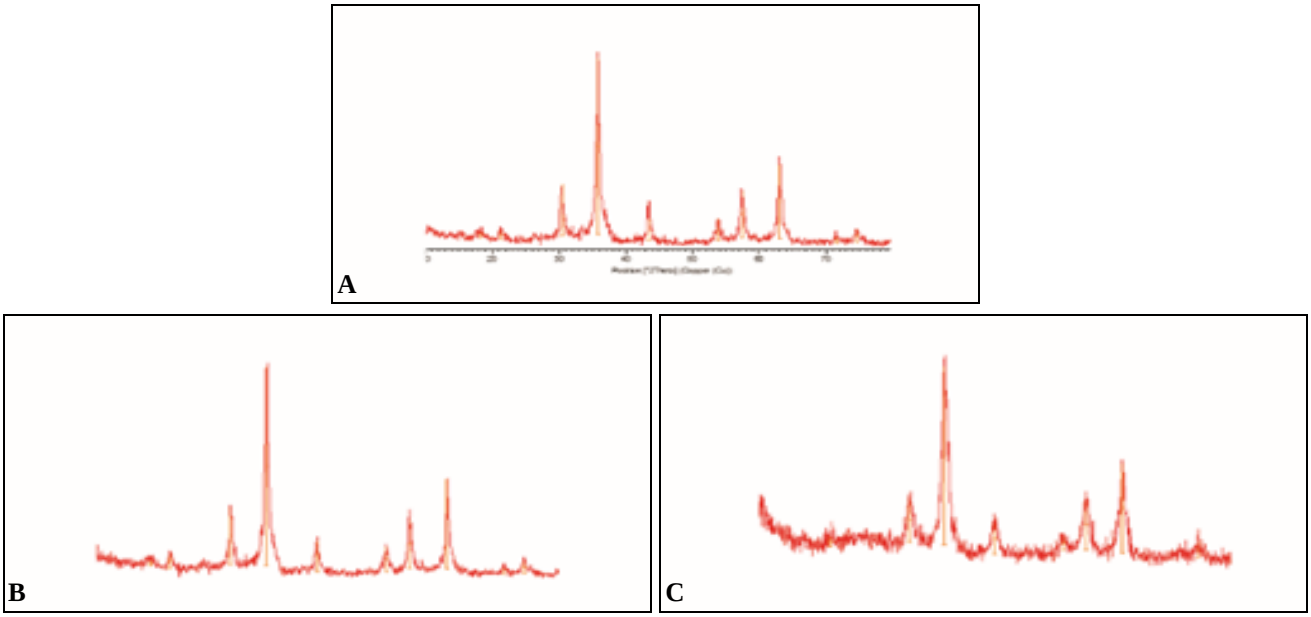


**FIG. 2: XRD DIFFRACTION PATTERN OF $Fe_3O_4$ (A), $Fe_3O_4$@$SiO_2$(B) AND $Fe_3O_4$@$SiO_2$@L-valine (C).**

**SEM Study:** Scanning electron microscopy (SEM) is an appropriate approach for characterizing surface morphology and dimension of the MNPs. The SEM image corresponding to the $Fe_3O_4$@$SiO_2$@L-valine is presented in **Fig. 3,** which displays relatively uniform-sized particles with nearly spherical shape and with a mean particle dimension of 15-30 nm.

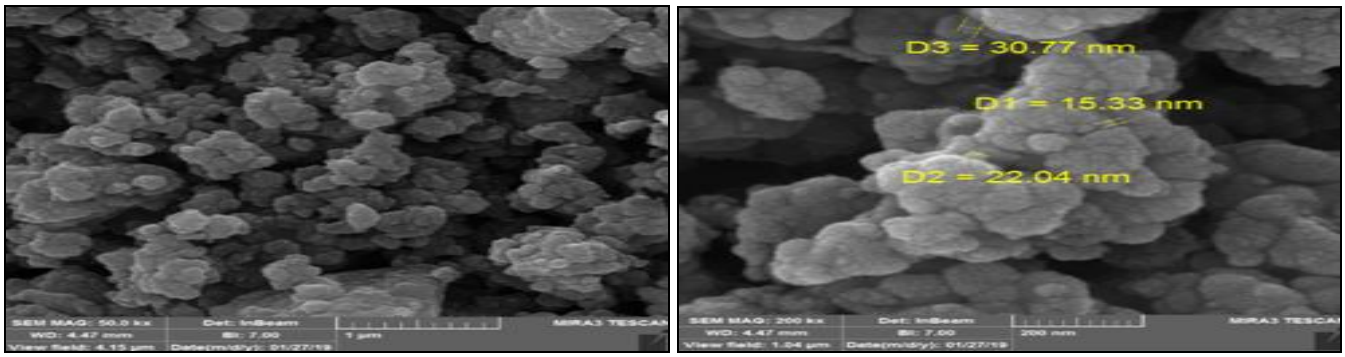


**FIG. 3: SEM IMAGES OF $Fe_3O_4$@$SiO_2$@L-valine MNPs**

**EDXA Study:** EDXA was utilized to provide some information on the elemental analysis corresponding to the $Fe_3O_4$@$SiO_2$@L-valine surface. Therefore, Fe, O, Si, C, and N were identified according to the outcomes presented in **Fig. 4**. The existence of nitrogen, carbon and oxygen signals in

the EDXA spectrum showed that L- valine was deposited on the $Fe_3O_4$@$SiO_2$ MNPs surface. Based on the above analysis, it can be recognized that the $Fe_3O_4$@$SiO_2$@L-valine MNPs have been effectively synthesized.

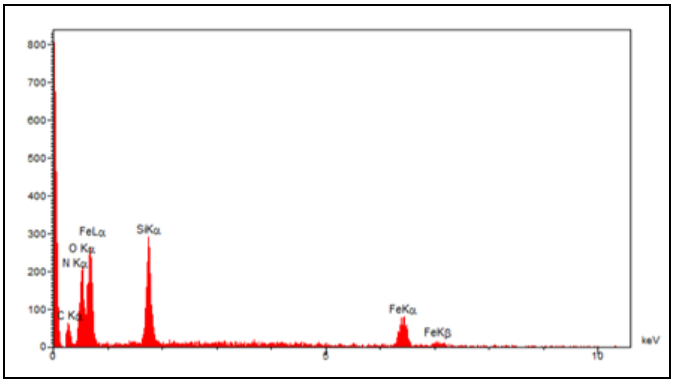


**FIG. 4: EDXA SPECTRUM OF $Fe_3O_4$@$SiO_2$@L-valine MNPs**

**Magnetic Study:** The magnetic properties of the $Fe_3O_4$ (a), $Fe_3O_4$@$SiO_2$(b), and $Fe_3O_4$@$SiO_2$@L-valine MNPs (c) were assessed by a vibrating sample magnetometer (VSM) at ambient temperature **Fig. 5**. The hysteresis curve permits designation of the saturation magnetization (Ms), coercivity (Hc), and remanent magnetization (Mr). The amounts of saturation magnetization (Ms) for (a) and (b) are almost 53 and 20.48 emu/g, respectively. Compared to the naked $Fe_3O_4$ MNPs, the saturation magnetization of $Fe_3O_4$@$SiO_2$and $Fe_3O_4$@$SiO_2$@L-valine is clearly reduced because of the additional mass of silica shell and valine layer. However, $Fe_3O_4$@$SiO_2$@L-valine can be isolated from the solution with a suitable magnet.

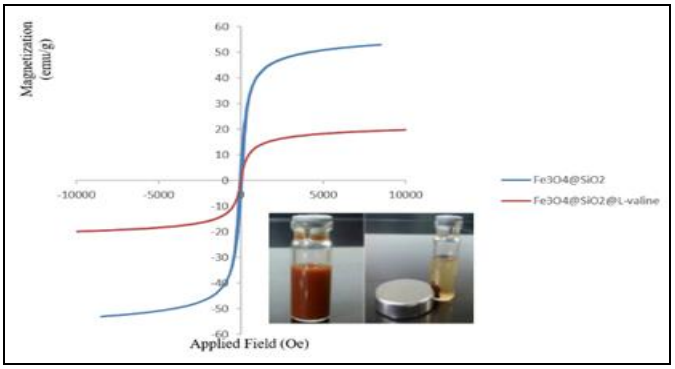


**FIG. 5: THE MAGNETIC HYSTERESIS LOOPS OF $Fe_3O_4$@$SiO_2$ and$Fe_3O_4$@$SiO_2$@L-valine**

**Synthesis and Characterization of Ligand:** 2-(2-methoxyphenyl)-2,3-dihydro-1H-perimidine ligand was prepared through condensation reaction of 1,8-diaminonaphthalene and 2-methoxybenzaldehyde (**Scheme 2**). To assess the need of the relating catalyst, a blank reaction of 1,8-diamino-naphthalene (1 mmol) and 2-methoxybenzaldehyde (1 mmol) was carried out in $H_2O$ (5 mL) as a solvent that afforded no product following 48 h (checked using TLC); thus, we decided to carry out the reaction with $Fe_3O_4$@$SiO_2$@L-valine as a catalyst. The substrates reaction condition was optimized in diverse conditions with different solvents and different catalyst loading to achieve the maximum yield.

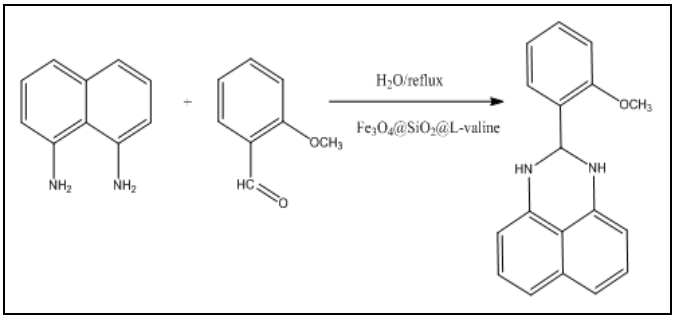


**SCHEME 2: SYNTHESIS OF 2-(2-METHOXYPHENYL)-2,3-DIHYDRO-1H-PERIMIDINE LIGAND**

Based on **Table 1**, the best yield was achieved using $H_2O$ as a solvent; different levels of catalyst were also studied. Table 1 displays the effect of various levels of catalyst on the product yield. The best result was achieved when 75 mg of $Fe_3O_4$@$SiO_2$@L-valine was utilized. As can be observed in Table 1, with enhancing levels of $Fe_3O_4$@$SiO_2$@L-valine nanocatalyst from 25 mg to 50 mg the recovery of reaction raised from 75% to 84% which caused a decrease in the reaction time. In contrast, enhancing the catalyst concentrations from 75 mg to 100 mg reduced the performance of the reaction from 90% to 63%. In the current research, $K_2CO_3$ was also utilized as a catalyst which indicated a much lower yield percentage (35%) with a longer reaction time.

Previously, the synthesis of this ligand and some other pyrimidine derivatives was reported by A. Mobinikhaledi *et al*., using nano-silica sulfuric acid (NSSA). The yield of the reaction was 83%, and in this research, we successfully achieved a higher yield and reported the single-crystal structure of this compound. The characterization of ligand was also performed using FTIR, $^{1}$H-NMR, $^{13}$C-NMR, and UV-visible. The X-ray structure corresponding to the ligand is presented in **Fig. 6**. Chosen peak length and angels are found in **Table 2**.

**TABLE 1: OPTIMIZATION OF THE REACTION CONDITION FOR THE PREPARATION OF PERIMIDINE LIGAND**

| Entry | Catalyst (mg) | Solvent | Time (min) | Yield (%) |
|---|---|---|---|---|
| 1 | $Fe_3O_4$@$SiO_2$@L-valine (25) | $H_2O$ | 180 | 75 |
| 2 | $Fe_3O_4$@$SiO_2$@L-valine (25) | EtOH | 240 | 63 |
| 3 | $Fe_3O_4$@$SiO_2$@L-valine (25) | $CH_3CN$ | 210 | 53 |
| 4 | $Fe_3O_4$@$SiO_2$@L-valine (50) | $H_2O$ | 180 | 84 |
| 5 | $Fe_3O_4$@$SiO_2$@L-valine (75) | $H_2O$ | 180 | 90 |
| 6 | $Fe_3O_4$@$SiO_2$@L-valine (100) | $H_2O$ | 180 | 63 |
| 7 | $K_2CO_3$ (75 mg) | $H_2O$ | 720 | 35 |

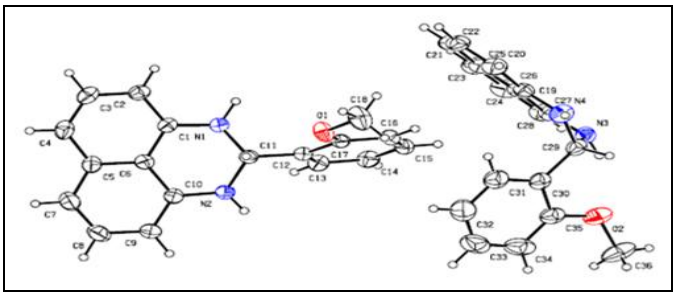

**FIG. 6: UNIT CELL OF LIGAND**

**TABLE 2: SELECTED BOND LENGTH AND ANGLES OF LIGAND**

| Bond (Å) | | Angles (°) | |
|---|---|---|---|
| O1-C17 | 1.381(3) | C17-O1-C18 | 117.7(2) |
| O1-C18 | 1.421(3) | C35-O2-C36 | 118.5(3) |
| O2-C35 | 1.370(4) | C1-N1-C11 | 114.3(2) |
| O2-C36 | 1.428(3) | C1-N1-H1A | 114(2) |
| N1-C1 | 1.403(3) | C11-N1-H1A | 111(2) |
| N1-C11 | 1.460(3) | C29-N4-H4A | 116(2) |
| C32-H32 | 0.9300 | C2-C1-N1 | 123.3(2) |
| C33-C34 | 1.369(6) | C2-C1-C6 | 120.1(2) |
| C33-H33 | 0.9300 | C3-C4-H4 | 119.7 |
| C34-C35 | 1.382(5) | C5-C4-H4 | 119.7 |
| C34-H34 | 0.9300 | C4-C5-C6 | 118.1(2) |

In the $^1$H-NMR spectra corresponding to ligand **Fig. 7**, a singlet peak was observed at 3.84 ppm corresponding to the aliphatic ($OCH_3$) group, while the signal of aromatic protons was seen between 7.58 and 7.00 ppm. The signal of amine groups (N-H) is found at 5.75 ppm, and the signal of aliphatic proton placed between the two amine groups was observed at 5.48 ppm. **Fig. 8** indicates the $^{13}$C-NMR spectra corresponding to the ligand. As expected, in the $^{13}$C-NMR spectra corresponding to this ligand, a peak at 59.50 ppm was assigned to the newly C-N nuclei, which proved the production of the ligand and the $OCH_3$ group appeared at 55.54 ppm. As can be seen in **Fig. 8**, the carbons of aromatic rings were also observed between 156.94 and 104.31 ppm **Fig. 8**.

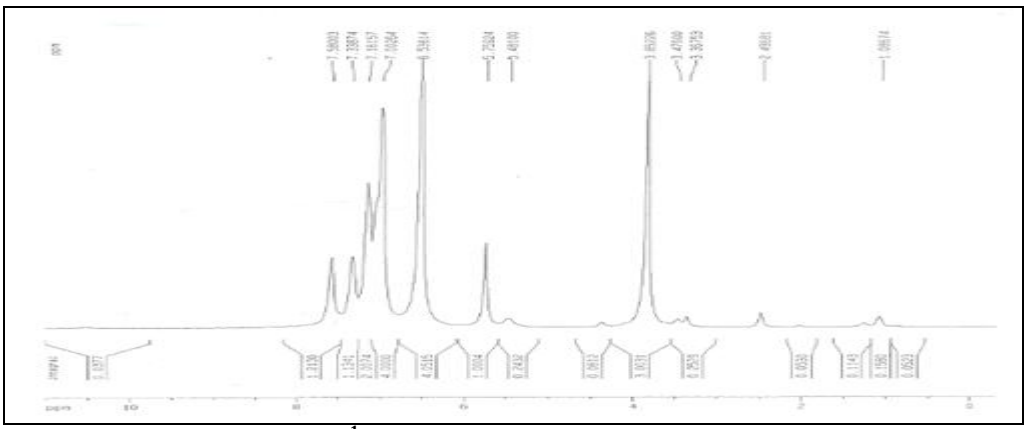

**FIG. 7: $^1$H-NMR SPECTRUM OF LIGAND**

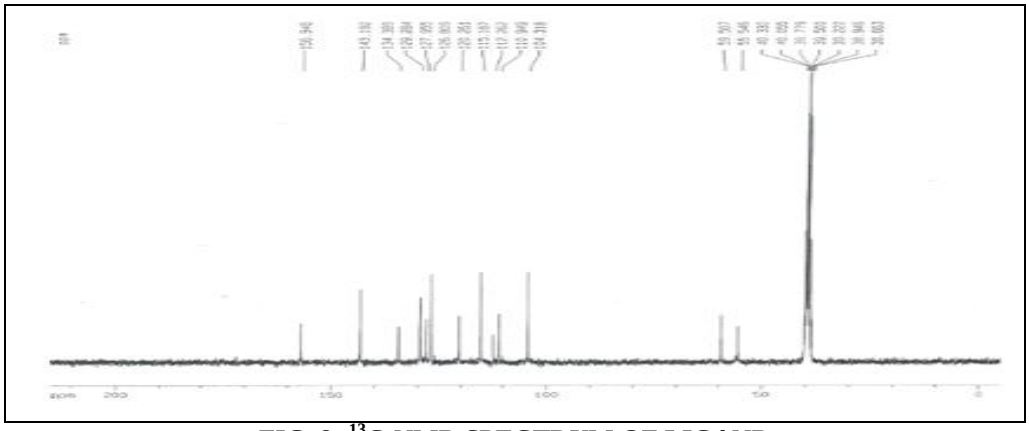

**FIG. 8: $^{13}$C-NMR SPECTRUM OF LIGAND**

In the FTIR spectrum of pyrimidine ligand, a broad peak seen in 3391 $cm^{-1}$, C-H aromatic, and C-H aliphatic signals were observed in 2927 and 2800 cm-1, respectively. The bands in the range of 1509-1602 $cm^{-1}$ appeared because of the C=C aromatic, while the peak corresponding to C-N was observed in 1300 $cm^{-1}$.

**Characterization of Metal Complexes:** In the Table below physical properties of metal complexes are presented.

**TABLE 3: PHYSICAL PROPERTIES OF LIGAND AND ITS METAL COMPLEXES**

| Compounds | M.W. (g/mol) | Yield (%) | Color | M.P. (°C) |
|---|---|---|---|---|
| L | 275 | 90 | Brown | 135-137 |
| CuL | 455 | 85 | Dark green | 110-112 |
| CoL | 450 | 72 | Blue | 105-107 |
| NiL | 450 | 70 | Pale green | 120-122 |

In the FTIR spectra corresponding to all the metal complexes, the N-H peak vanished, which showed that the ligand coordinated to the metal ions with nitrogen atom. The FTIR spectra also represent the M-N and M-O stretching peaks appearing between 626 and 684 $cm^{-1}$. The C-H aromatic and C-H aliphatic stretching frequencies we removed to the lower wavenumbers when proved to free ligand. Strong peaks in the range of 3300-3500 $cm^{-1}$ showed the presence of H2O in the structure of all complexes.

Electronic spectra corresponding to complexes were obtained in DMSO, and the main spectral data are listed in **Table 4**. Based on the data, the tetrahedral geometry is proposed for all the metal complexes with a coordination number of four.

**TABLE 4: UV-VISIBLE DATA OF LIGAND AND METAL COMPLEXES**

| Compound | Transitions | Assignment | Geometry |
|---|---|---|---|
| L | 270, 350 nm | $\pi \rightarrow \pi^*, n \rightarrow \pi^*$ | - |
| CuL | 260, 400, 440 nm | $\pi \rightarrow \pi^*, n \rightarrow \pi^*, T_2 \rightarrow E$ | Tetrahedral |
| CoL | 250, 330, 580 nm | $\pi \rightarrow \pi^*, n \rightarrow \pi^*, A_2 \rightarrow T_1, A_2 \rightarrow T_2$ | Tetrahedral |
| NiL | 300, 410 nm | $n \rightarrow \pi^*, T_1 \rightarrow T_2$ | Tetrahedral |

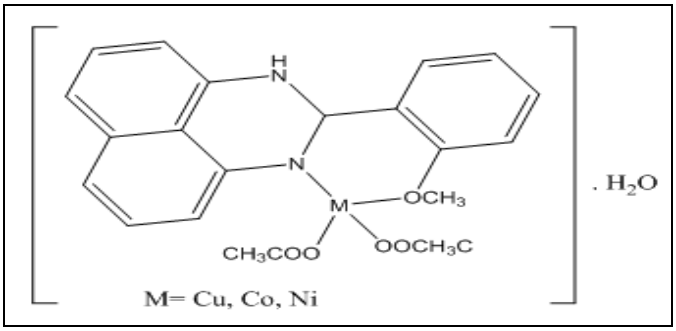


**FIG. 9: PROPOSED STRUCTURE OF METAL COMPLEXES**

The mass spectra corresponding to the metal complexes were obtained at ambient temperature to approve the stoichiometry of metal chelates as examined above. The molecular ion band corresponding to CuL, CoL and NiL complexes appeared at m/z= 455, 450 and 450, respectively which is equal to the molecular weight for the complexes. The suggested structure for the metal complexes is presented in **Fig. 9**.

**Recovery and Reusability of the Catalyst:** The recoverability of $Fe_3O_4$@$SiO_2$@L-valine nano-catalyst was studied for the reaction of 1,8-diaminonaphthalene and 2-methoxybenzaldehyde under optimal conditions. At the end of the reaction, the catalyst was recycled with an external

magnet and washed with ethanol, and dried at a temperature of 60 °C. The catalytic behavior corresponding to $Fe_3O_4$@$SiO_2$@L-valine MNPs was studied for another five cycles, and outcomes indicated that the catalytic behavior was approximately reduced from 90 to 80 percent, a decrease by10 percent following 5 cycles, as can be observed in **Fig. 10**. To explain, this catalyst was not fully recycled using an external magnet, or there probably was chemical poisoning of the catalyst surface over the reaction.

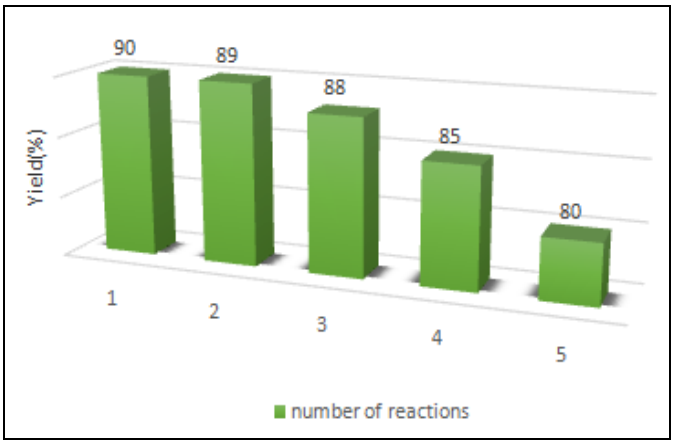


**FIG. 10: RECOVERABILITY OF $Fe_3O_4$@$SiO_2$@L-valine IN THE SYNTHESIS OF PERIMIDINE LIGAND**

**Antibacterial Activity:** Antibacterial behavior of the ligand, its complexes, and standard antibiotic drug (tetracycline) were studied against *Escherichia coli*, *Serratia maracescens* (gram-negative bacteria), *Bacillus sabtilis*, and *Staphylococcus* aureus, (gram-positive bacteria) with Muller Hinton agar media through disk diffusion technique. The antibacterial property of the prepared materials is represented in Table 5. The antibacterial property was assessed via the measurement of the inhibition zone diameter corresponding to all bacteria strains. According to the data presented in **Table 5**, the prepared compounds were more efficient against *E. coli* with inhabitation zone of 14, 17, 15, and 14 mm for ligand, CuL, CoL, and NiL, respectively.

It is obvious that metal chelates have more biological property compared to the parent ligand. Such enhanced activity corresponding to the metal chelates can be described according to Overtone's concept and chelation theory [13-16]. On chelation, the polarity corresponding to the metal ion is decreased to a greater extent because of overlapping the orbital of ligand and partial sharing of the positive charge corresponding to the metal ion with donor groups. Additionally, it enhances the delocalization of p-electrons through the chelate ring and improves the complex lipophilicity. This enhanced lipophilicity increases penetrating the complexes into lipid membranes and blockage of the metal binding places in the microorganisms enzymes.

**TABLE 5: ANTIBACTERIAL ACTIVITY OF SYNTHESIZED COMPOUNDS AS INHABITATION ZONE DIAMETER (mm)**

| Compounds | *B. subtilis* | *S. aureus* | *E. coli* | *S. marcescen* |
|---|---|---|---|---|
| L | 12 | 10 | 14 | 12 |
| CuL | 15 | 14 | 17 | 15 |
| CoL | 14 | 15 | 15 | 14 |
| NiL | 14 | 12 | 14 | 14 |
| DMSO | 0 | 0 | 0 | 0 |
| Tetracycline | 10 | 17 | 12 | 12 |

**Experimentation:** All reagents and solvents were purchased from Sigma Aldrich (St. Louis, MO, USA) and Merck (Darmstadt, Germany) companies and were utilized with no additional purification. Fourier-transform infrared spectra (FTIR) of all the prepared materials were achieved in the region of 400–4000 $cm^{-1}$ by means of a Shimidzo 300 spectrometer using potassium bromide pellets. An Electrothermal 9200 apparatus was used to record melting points without any correction. UV-visible spectra were recorded by means of a Cary 100 spectrophotometer in DMSO solutions. $^1$H-NMR (Nuclear magnetic resonance) spectra corresponding to the ligand were carried out on a Brucker AMX 300 MHz spectrometer in DMSO $d_6$ with tetramethylsilane (TMS) as an internal standard. The mass spectra were obtained at 70 eV at the temperature of 230 °C with Agilent technologies. The characterization of the crystal structure of the magnetic nanoparticle catalyst was performed using an X-ray diffractometer (STOE, STADIP) equipped with Cuk α irradiation (λ=1.54 angstrom) in the 2 θ scanning range of 10-80, and particle size (PS) was computed using Deby-Scherer's formula. The shape and surface morphology of MNPs were examined by means of a scanning electron microscope (SEM, KYKY-EM3200). The magnetic property was explained using a vibration sample magnetometer (VSM, BHV-S5) by means of the external magnetic field between 10 kOe. A thin layer chromatography (TLC) on silica gel polygram SILG/UV 254 nm plates was used to check the reactions completion.

**Synthesis of $Fe_3O_4$ MNPs:** The overall process for producing the nanocatalyst is shown in **Fig. 1**. $Fe_3O_4$ MNPs were synthesized through chemical co-precipitation of ferric and ferrous salts as explained in the literature. For this purpose, $FeCl_3 \cdot 6H_2O$ (2 mmol) and $FeCl_2 \cdot 4H_2O$ (1 mmol) were poured in 100 mL distilled water under magnetic stirring. Following 30 min, the solution was heated to the temperature of 90 °C under nitrogen atmosphere. Next, the NaOH solution (55 mL, 3M) was poured dropwise to a reaction mixture until achieving pH 11. Following that, sodium citrate (11g/100mL) was poured to the resulted reaction mixture with constant stirring at ambient temperature for 12 h. Then, the black sediment was separated from the reaction mixture using a suitable magnet. Lastly, the solid material achieved was rinsed with de-ionized water and ethanol several times to eliminate the residual impurities.

**Synthesis of $Fe_3O_4$@$SiO_2$:** The $SiO_2$ coated-$Fe_3O_4$ was synthesized through the Stober technique. $Fe_3O_4$ MNPs (1 g) was added in a mixture containing 20 mL ethanol and 50 mL distilled water. In the next phase, concentrated ammonia solution (25%) was poured dropwise in an ultrasonic bath for half an hour. Next, Then tetraethyl orthosilicate (TEOS) (0.5 ml) was poured dropwise while it was agitated for 24 h at ambient temperature. The resulted solid was magnetically isolated and was rinsed several times with water and ethanol, and lastly dried in a vacuum oven at the temperature of 60 °C for 10 h.

**Synthesis of $Fe_3O_4$@$SiO_2$@L-valine:** As much as 5 mmol of L-valine dissolved in 20 mL of ethanol was poured into a magnetically stirred mixture of the synthesized $Fe_3O_4$@$SiO_2$ (1 g) and the mixture was sonicated for half an hour and then refluxed at the temperature of 70 °C for 12 h. The resulted solid was magnetically isolated from the solution and was rinsed several times with water and ethanol, and lastly dried in a vacuum oven at the temperature of 60 °C for 12 h.

**Synthesis of 2-(2-methoxyphenyl)-2,3-dihydro-1H-perimidine (L):** $Fe_3O_4$@$SiO_2$@L-valine (3 mg) was dispersed in 10 mL distilled water and poured into a mixture containing 1,8-diamino-naphthalene (1 mmol) and 2-methoxybenzaldehyde (1 mmol). The reaction mixture was refluxed at room temperature and monitored with TLC. At the end of the reaction, the catalyst was isolated with an external magnet. Then, the solvent was evaporated under reduced pressure and lastly dried in a vacuum oven at the temperature of 60 °C for 5 h.

**Synthesis of Metal Complexes:** All the complexes were produced through the same method. The solution of a ligand in ethanol (1 mmol) was combined with $M(CH_3COO)_2.XH2O$ and refluxed at the temperature of 70 °C for 2-4 h. Next, the precipitate was filtered, rinsed with ethanol and water, and lastly, dried in a desiccator under vacuum condition.

**Antibacterial Study:** A wide range of laboratory approaches can be utilized to study in vitro antibacterial behavior of the materials. In the current research, disc diffusion technique was employed. *Escherichia coli* (ATCC: 25922) and *Serratia maracescens* (ATCC: 13880) were utilized as gram-negative bacteria, while *Bacillus sabtilis* (ATCC: 6633) and Staphylococcus aureus (ATCC: 6838) were utilized as gram-positive micro-organisms.

These experiments were carried out through the procedure explained in the guidelines of the National Committee for Clinical Laboratory Standards (NCCLS) [17]. Accordingly, the solution of the produced compounds was prepared at 20 mg/mL in DMSO under sterile conditions. Tetracycline was utilized as a standard antibiotic medicine. Suspensions of each bacteria strain were prepared by culturing them in Muller Hinton agar (MHA) media for 24 h to achieve almost $1.5 \times 10^8$ colony forming units (CFU) per ml. Paper discs of 8 mm diameter were soaked separately in a constant level (100 µg/ml) of the compounds and were then permitted to dry. In the next step, the dried discs were located in the inoculated agar surface and incubated at the temperature of 35 °C for 18-24 h. The anti-bacterial feature was shown by the existence of clear inhibition zones around each disc. Each experiment was performed three times.

**X-Ray Data Collection and Refinement of Crystal Structure of Ligand:** Crystals of 2-(2-methoxyphenyl)- 2, 3-dihydro-1H-perimidine (L)

were grown through slow evaporation from ethanol solution. The X-ray diffraction analysis was performed on STOE IPDS 2T diffractometer with graphite monochromated Mo Kα (λ = 0.71073 Å) irradiation. The ligand's crystal structure achieved following 10 days was analyzed using X-ray crystallography (CCDC code: khc1411h comprising the supplementary crystallographic data). The crystal data and structure refinement of the ligand is presented in **Table 6**. The refinement was carried out using SHELXL 97. The analysis of structure was performed by direct technique. These data can be seen from the Cambridge Crystallographic Data Center at www.ccdc.com.ac.uk/data-request/cif.

**TABLE 6: CRYSTAL STRUCTURE DATA OF LIGAND**

| | |
|---|---|
| Empirical formula | $C_{18}H_{16}N_2O$ |
| Formula weight | 276.33 |
| System | Triclinic |
| Color/shape | Brown/plate |
| Space group | P -1 |
| a (A˚ ) | 10.323(2) |
| b (A˚ ) | 10.875(2) |
| c (A˚ ) | 14.007(3) |
| α (°) | 99.39(3) |
| B (°) | 100.74(3) |
| γ (°) | 110.68(3) |
| T (k) | 298(2) |
| V (A˚ $^3$) | 1399.8(5) |
| Z | 4 |
| $D_{cal}$ (Mg/m$^3$) | 1.311 |
| Crystal size (mm) | 0.45 |

**CONCLUSION:** An easy and effective technique has been reported for synthesizing new 2-(2-methoxyphenyl)-2,3-dihydro-1H-perimidine ligand via condensing 1,8-diaminonaphthalene and 2-methoxy benzaldehyde with $Fe_3O_4$@$SiO_2$@L-valine nanoparticles under optimal conditions. The protocol provides several advantages such as a green solvent system, mild reaction conditions, greater yields, recoverability of the catalyst, and shorter reaction time. The characterization of $Fe_3O_4$@$SiO_2$@L-valine was performed by FT-IR, XRD, SEM, EDXA, TEM, and VSM. The metal complexes were synthesized through the reaction of ligand and Cu(II), Co(II), and Ni(II) in excellent yields. Lastly, the antibacterial behavior of the prepared materials was studied against four microorganisms. Findings revealed that the coordination materials had more antibacterial behavior compared to the parent ligand.

**ACKNOWLEDGEMENT:** We would like to thank Islamic Azad University, Tehran North Branch, for partial financial support.

**CONFLICTS OF INTEREST:** Nil

## REFERENCES:

1. Filho JBMR, Santos PR, Vale JA, Faustino WM, Farias DS, Brito HF, Felinto MCFC and Teotonio EES: J Braz Chem Soc 2017; 28(12): 5053.
2. Alinezhad H, Ahmadi A and Hajiabbasi P: J Chem Sci 2019; 131.
3. Mandoli A: Molecules 2016; 21: 1174.
4. Caminade AM and Laurent R: Coord Chem Rev 2019; 389: 59.
5. Akhavan M, Foroughifar N, Pasdar H, Khajeh-Amiri A, Bekhradnia A: Transit Met Chem 2017; 42(6): 543.
6. Le TXH, Cowan MG, Drobek M, Bechelany M, Julbe M and Cretin M: Nanomaterials 2019; 9: 641.
7. Afradi M, Foroughifar N, Pasdar H, Moghanian and H: RSC Adv 2016; 6: 59343.
8. Afradi M, Foroughifar N, Pasdar H and Moghanian Foroughifar N: Organometal Chem 2016. doi: 10.1002/aoc.3683.
9. Davoodi SD and Hedayati Saghavaz B: Biointerface Research in Applied Chemistry 2017; 7(6): 2249.
10. Gholami-Dehbalaei M, Foroughifar N, Khajeh-Amiri A and Pasdar H: J Chin Chem Soc 2018, 1.
11. Gholami-Dehbalaei M, Foroughifar N, Pasdar H, Khajeh-Amiri A: New J Chem 2018; 42: 327.
12. Gade VB, Goswami A, Varma RS, Shelke SN and Gawande MB: Nanomaterials 2018; 8: 246.
13. Hedayati-Saghavaz B, Pasdar H and Foroughifar N: Biointerface Research in Applied Chemistry 2016; 6(6): 1842.
14. Khadivi R, Pasdar H, Foroughifar N and Davallo M: Biointerface Research in Applied Chemistry 2017; 7(6): 2238.
15. Pasdar H, Hedayati-Saghavaz B, Foroughifar N, Davallo M: Molecules 2017; 22: 2125.
16. Siabi S, Pasdar H, Foroughifar N, Davallo M and Fazaeli R: Biointerface Research in Applied Chemistry 2018; 8(4): 3418.
17. Wang X, Xie X, Cai Y, Yang X, Li J and Li Y: Molecules 2016; 21: 340.

**How to cite this article:**
Siabi S, Pasdar H, Foroughifar N, Davallo M and Fazaeli R: Preparation and characterization of $Fe_3O_4$@$SiO_2$@L-valine nanoparticles as an effective and novel nanocatalyst for the synthesis of perimidine derivative under mild conditions. Int J Pharm Sci & Res 2021; 12(4): 2385-93. doi: 10.13040/IJPSR.0975-8232.12(4).2385-93.